



Fabrication and characterization of zeolite bulk body containing mesopores and macropores using starch as pore-forming agent

Masako Uematsu, Kento Ishii, Sadaki Samitsu, Izumi Ichinose, Naoki Ohashi, David Berthebaud, Jean-François Halet, Takamasa Ishigaki, Tetsuo Uchikoshi

► To cite this version:

Masako Uematsu, Kento Ishii, Sadaki Samitsu, Izumi Ichinose, Naoki Ohashi, et al.. Fabrication and characterization of zeolite bulk body containing mesopores and macropores using starch as pore-forming agent. *Advanced Powder Technology*, 2022, 10.1016/j.appt.2022.103626 . hal-03689132

HAL Id: hal-03689132

<https://cnrs.hal.science/hal-03689132>

Submitted on 7 Jun 2022

HAL is a multi-disciplinary open access archive for the deposit and dissemination of scientific research documents, whether they are published or not. The documents may come from teaching and research institutions in France or abroad, or from public or private research centers.

L'archive ouverte pluridisciplinaire **HAL**, est destinée au dépôt et à la diffusion de documents scientifiques de niveau recherche, publiés ou non, émanant des établissements d'enseignement et de recherche français ou étrangers, des laboratoires publics ou privés.

**Fabrication and characterization of zeolite bulk body containing mesopores and macropores
using starch as pore-forming agent**

Masako Uematsu^{a,b,c*}, Kento Ishii^b, Sadaki Samitsu^d, Edhuan Bin Ismail^b, Izumi Ichinose^b,
Naoki Ohashi^{b,c}, David Berthebaud^c, Jean-François Halet^c, Takamasa Ishigaki^{e,f}, Tetsuo Uchikoshi^{a,b,c,f*}

^a Graduate School of Chemical Science and Engineering, Hokkaido University,
Sapporo, Hokkaido 060-8628, Japan.

^b Research Center for Functional Materials, National Institute for Materials Science,
Tsukuba, Ibaraki 305-0047, Japan.

^c CNRS–Saint-Gobain–NIMS, IRL 3629, Laboratory for Innovative Key Materials and Structures (LINK),
National Institute for Materials Science, Tsukuba, Ibaraki 305-0044, Japan.

^d Microstructural Characterization Platform, National Institute for Materials Science,
Tsukuba, Ibaraki 305-0047, Japan.

^e Department of Chemical Science and Technology, Hosei University, Koganei, Tokyo 184-8584, Japan.

^f Research Center for Micro-Nano Technology, Hosei University, Koganei, Tokyo 184-0003, Japan.

Corresponding author: Tetsuo Uchikoshi

(E-mail: UCHIKOSHI.Tetsuo@nims.go.jp / UEMATSU.Masako@nims.go.jp,

Phone: +81-298-54-2460, Fax: +81-298-24-7843)

Abstract

Zeolite bulk bodies containing macropores, mesopores, and micropores were prepared and characterized using ZSM-5 raw powder as the starting material. Starch powder was selected as a pore-forming agent and the internal porous structure was controlled by using the property that starch particles form a network structure by

heat treatment. The presence of mesopores was characterized by N₂ gas adsorption/desorption measurement, and the macroporous structure was observed by the 3D-image analysis of hundreds of cross-sectional images in the depth direction by a confocal laser fluorescent microscope using the liquid immersion method. The observation method demonstrated that it is possible to observe structures of several microns size in the three dimensions. The compressive strength and N₂ gas permeability of the bulk samples depended on the sample structure; bulk bodies with a compressive strength comparable to that of general concrete were created. The network structure of the starch pore-forming agent was effective in creating a continuous macroporous structure. The bulks could be used in applications such as novel catalyst carriers and filters, and combining functional nanoparticles.

Keywords: ZSM-5, starch, mesoporous material, zeolite bulk, three-dimensional observation

1. Introduction

Zeolites are microporous crystalline aluminosilicates known as molecular sieves that have been widely used in industry as adsorbents, catalysts, and ion exchangers. The hydrothermal method is commonly used for the synthesis of zeolites, which are generally obtained as powders consisting of nano- to micron-sized crystals [1-3]. The molecular sieving ability of zeolites depends on their crystalline structure containing pores and cavities of molecular dimension. Efforts have long been made to increase the pore size of zeolite crystal units due to the potential capacity of chemical processes that require larger pore spaces as reaction fields. Consequently, the synthesis of extra-large pore zeolite has been attempted [4-9], leading to the synthesis of

ITQ-37 having a 30-membered ring. However, the diameter of largest-free-sphere of zeolite units listed in the IZA database [10] is still less than 10 Å. For now, the reactants or supported materials on the zeolites are limited in terms of cavity size. Mesoporous materials, such as MCM-41, are also known as zeolite-like materials with nanoscale pore size structures [3,11-13]. However, due to their low crystallinity, their ability as acid catalysts is lower than that of the zeolites.

Zeolite bulks containing mesopores and macropores have great potential to improve the capabilities of larger molecular reactors. S. Zou *et al.* reported the synthesis of a hierarchically porous zeolite using a polyurethane form template [14], and M. Anderson *et al.* proposed a biomineralization method using diatoms [15]. However, they did not mention the mechanical strength. The handling availability with a sufficient mechanical strength is an important factor for practical use as a bulk body. E. Igi *et al.* synthesized a porous zeolite bulk body by one-pot hydrothermal method and reported that it had sufficient mechanical strength for machining. [16, 17]. Here, we propose a new processing method for producing a porous zeolite bulk body that contains micropores, mesopores, and macropores and that has sufficiently high mechanical strength for handling. Hybrid materials consisting of zeolites and functional particles are expected to be used as novel catalysts or purification filters. Mesopore will be effective in supporting functional nanoparticles. Continuous macropores will be essential for the smooth flow of gas or liquid that needs to be treated.

Starch has been used as a pore-forming agent, and a hierarchical porous structure was introduced into the zeolite bulks [18-20]. Starch forms a gel with a α -starch network when heated with water. The α -starch gel turns into solidified β -starch after a cooling process, thus keeping the network structure. This starch property is appropriate for a pore-forming agent to make a networked porous structure [20]. In this study, rice starch

was used as a pore-forming agent, and a hierarchical porous structure was introduced into the zeolite bulks. We investigated the morphological changes of the pore structure in the zeolite bulk body involved with the gelation treatment of the pore-forming agent. In order to reveal the hierarchically pore structure, it is necessary to investigate the existence of micropores with a diameter of less than 2 nm, mesopores with a diameter of 2-50 nm, and macropores with a diameter of more than 50 nm. Micropores and mesopores can be generally characterized from N₂ gas adsorption/desorption isotherms [21,22]. For macropores, we attempted the direct observation of the pore structure using a confocal laser fluorescent microscope (CLFM) employing the liquid immersion method. It is a high-resolution three-dimensional observation method which was developed to characterize the defects in a ceramic green-body and granules [23,24]. The liquid immersion method is also an internal structure observation technique that can be applied to a system in which the material is transparent to the observation light and has a little optical anisotropy. A ceramic compact or a bulk body becomes transparent when an immersion liquid having the close refractive index to the raw material of the sample is permeated into the open pores, thus reducing light scattering on the surface of the raw material. Observation inside the samples becomes available using a fluorescent microscope by dissolving a small amount of fluorescent agent in the immersion liquid. In our investigations, we used this technique to characterize the porous structure in the bulk zeolite. Finally, the mechanical strength and gas permeation rate of the bulk body were evaluated and associated with the pore structure.

2. Experimental procedures

Commercially-available ZSM-5 zeolite powder (HSZ-840HOA, Tosoh Corp., Japan) was used as the

starting material. The particle size distribution of the ZSM-5 powder measured by the DLS method (Nanotrac UPA-UT, Nikkiso Co., Ltd.) is shown in Fig. S1. Aqueous colloidal silica (Snowtex ST-S, Nissan Chemical Corp., Japan) with the average particle size of 9 nm, containing 30 wt% SiO₂, was used as a binder. The ZSM-5 powder was added to the aqueous colloidal silica so that the weight ratio of zeolite to silica was 2:1. The slurry was ball-milled at 30 rpm for 24 hours using a zirconia ball medium (2- 10 mm diameter). Rice starch powder (Sigma-Aldrich Co. LLC) with the particle size range of 2.0- 8.0 μm was added to the slurry as a pore-forming agent in the amount of 20 wt% or 0 wt% vs. the solid contents in the slurry. The starch was mixed and dispersed in the slurry using a planetary centrifugal mixer (ARE-310, THINKY Corp., Japan) at 2000 rpm for 5 minutes. The slurry was cast into acrylic molds with a 16 mm diameter and steamed in water vapor at 80 °C for 10 minutes to gelatinize the starch or just dried with no heating. The green bodies were treated in an autoclave for 24 hours in steam at 180 °C without direct contact with water as shown in Fig. 1 to bind the zeolite particles by a surface reaction between the colloidal silica and the zeolite. The consolidated bodies were then thermally treated in air at 450 °C for 24 hours to remove the starch. Finally, three porous zeolite bulk bodies formed by different processes were obtained. In other words, the following three types of samples were prepared as sample (1); sample without starch, sample (2); sample with starch and no heat-treatment, and sample (3); sample with starch and heat-treatment. The schematic illustrations of the expected internal structure of each sample are shown in Fig. S2.

The crystal structures of the raw zeolite powder and the bulk samples were identified by an X-ray powder diffraction measurement (Miniflex600, Rigaku) with CuKα radiation. The pore size distribution in the mesoporous region was characterized by a nitrogen-gas adsorption/desorption measurement using a surface

area and pore distribution size analyzer (BELSORP-II, MicrotracBEL). The Barrett-Joyner-Halenda (BJH) method was applied to the desorption isotherm to calculate the pore size distribution. The BJH method is based on the Kelvin equation, which assumes a system of open-ended, cylindrical mesopores. The capillary radius can be calculated when capillary condensation occurs from the Kelvin equation [21]. The specific surface area was calculated from the α_s -plot since the Brunauer-Emmet-Teller (BET) theory is not applicable to microporous materials [22]. The fracture surface of the bulk bodies was observed by scanning electron microscopy (JSM-6500F, JEOL). The internal structure of the bulk bodies was observed by a confocal scanning laser fluorescence microscope (TCS-SP5, Leica Microsystem) using the liquid immersion method [23,24] as schematically illustrated in Fig. 2. The sample became transparent to visible light when the immersion liquid, which has the refractive index n close to that of the base material, permeated into the samples due to reducing of the reflection of light at the interface of the powder particles and the surrounding medium. The refractive index of the synthesized ZSM-5 is 1.48 [25], therefore, 1-methyl-2-francalboxyrate ($n = 1.48-1.49$) [26] was selected as the immersion liquid. The fluorescent agent, Rhodamine B, was dissolved in the immersion liquid before liquid permeation to distinguish between the open pores and zeolite bulk. The samples were fractured, then ground with an abrasive paper to a thickness of 200-500 μm before the liquid immersion. The internal microstructures of the samples were observed by confocal scanning laser fluorescence microscopy. Cross-sectional images of the sample from the surface to a depth of 65 μm were continuously obtained at intervals of 0.26 μm . The sliced images were binarized into the pore and base material phases, then these images were stacked to create a three-dimensional image using an image processing software (AVIZO, Thermo Fisher Scientific, Inc.). The density of the bulk bodies was measured by Archimedes' method using kerosene as the

solvent. The mechanical strength of the bulk bodies was evaluated by compressive strength tests using an autograph (AG-I, SHIMADZU, Corp.) based on Japanese industrial standards [27]. The samples were polished to a diameter of 12 mm and a height of 10 mm for the tests. Seven test pieces were used to measure the strength of each sample. The gas permeabilities of the samples were evaluated by a permeation membrane analyzer (PMA-601, SepraTek). A circular hole with a diameter of 6 mm was cut in the center of a round PET sheet with a diameter of 55 mm and a thickness of 110 μm . A sample with a diameter of 12 mm and a thickness of 2 mm was then fixed in the hole of the round PET sheet with epoxy resin. The sample fixed to the PET sheet was placed in the chamber of the analyzer. The amount of gas permeation per unit of time was measured by flowing 0.2 MPa of N_2 gas from one side of the sample as shown in Fig. 3.

3. Results & Discussion

Hard, crack-free bulk samples were successfully fabricated. A zeolite bulk body with starch heated is shown in Fig. 4. The other samples are also white lumps, suggesting that the starch has been completely removed. X-ray diffraction patterns of the raw ZSM-5 powder and the bulks are shown in Fig. 5. All peaks of the bulk samples were identified as peaks of the ZSM-5 phase. The results indicated that the bulk body maintained the crystal structure of the ZSM-5 zeolite through all the processes. The colloidal silica phase did not appear in the XRD probably because it remained as an amorphous phase.

The N_2 adsorption/desorption isotherms measured at 77 K are shown in Fig. 6. According to the IUPAC, the physisorption isotherm is grouped into six types [22]. Furthermore, Type I and Type IV have the sub-categories (a) and (b), respectively. The isotherm of the raw ZSM-5 powder is classified as type I(a), indicating

that it was a typical microporous material. On the other hand, the isotherms of the bulk bodies showed hysteresis loops which were provided by mesoporous adsorbents classified as Type IV(a). However, the isotherms of the bulk samples also indicated a steep uptake at a very low relative pressure the same as the raw material due to the micropore filling. In addition, the successive uptake of bulk's isotherms in the high relative pressure region revealed the presence of macropores. It suggests that bulk samples contained pores of various sizes not found in the raw zeolite powder, such as mesopores and macropores. There was no significant difference in the shape of the adsorption isotherm between the sample (1) and the sample (2). The sample (3) clearly increased the amount of adsorption at the same relative pressure. For example, the amount of adsorption at a relative pressure of around 1.0 was approximately 200 cm³(STP)/g for the sample (1) and the sample (2), while it was approximately 240 cm³(STP)/g for the sample (3).

The pore size distributions obtained from the BJH plots are shown in Fig. 7. Since the capillary condensation theory cannot be applied to pores below 2 nm, the BJH plot cannot provide micropore comparisons. However, it is effective for discussion about the mesopore region. All the bulk samples had a peak distribution at 7-9 nm, corresponding to mesopores, regardless of the addition of starch. It was also found that the sample (3) contained the largest volume of mesopores. The amount of mesopores did not significantly change between the sample (1) and sample (2). The results mean that mesopores would be formed between the zeolite particles in the bulk, and that they were increased by the starch network structure. The zeolite bulks with mesopores would be suitable for supporting functional nanoparticles. The specific surface area of the samples calculated by the α_s -plots was as follows: sample (1): 378 m²g⁻¹; sample (2): 375 m²g⁻¹; sample (3): 387 m²g⁻¹; ZSM-5 raw powder: 573 m²g⁻¹. The three bulk samples have very similar specific surface areas to

each other, and they were lower than that of the ZSM-5 raw powder. For the bulk sample, the contact between the particles leads to a lower surface area. The presence of the pore-forming agent did not contribute to the specific surface area because the amount of micropores was the dominant factor for the specific surface area of the bulk samples.

Macroporous structures were characterized by observation using a scanning electron microscope (SEM) and a confocal laser fluorescence microscope (CLFM). SEM images of the fracture surface at two different magnifications and CLFM images of the corresponding samples are shown in Fig. 8. The CLFM images were taken at a depth of 20 μm from the sample surface. Black spots on the CLFM images correspond to pores. The structural images obtained by the two observation methods are similar demonstrating the validity of this internal observation method. Cross-sectional images by CLFM revealed that the structure of the pores clearly changes with the addition of starch and its gelation process. No large pores were observed in the sample (1). On the other hand, large pores with a size of more than 5 μm were observed in the sample (2) and sample (3), and the two pore structures were different depending on the presence or absence of the heating process. The higher magnified SEM images revealed the existence of pores that have a size of less than 1 μm . The three-dimensional images of the macropores created from 173 sliced CLFM images per each sample are shown in Fig. 9. Conventional micro-X-ray CT is generally known as a three-dimensional observation method, but it is difficult to observe a pore structure of several microns in terms of resolution, except when using large synchrotron radiation facilities [28]. It was demonstrated that the CLFM method is excellent for facilitating the 3D high resolution observations. Results of the density measurement by Archimedes' method is shown in Table 1. As already mentioned, the sample (2) and the sample (3) had different macropore structures, but the

porosity measured by Archimedes' method was similar because the same amount of pore-forming agent was added.

The compressive strength of the zeolite bulk bodies is shown in Fig. 10. All the samples had a compressive strength above 25 MPa. The compressive strength of the bulks was more than that of general concrete for construction which has a strength of 24 MPa [29]. Igi *et al.* have reported that the machinable ZSM-5 bulk body has a bending strength of approximately 5 MPa [17]. The bending strength is said to be about one-fifth to one-seventh of the compressive strength in the case of concrete [30]. Assuming a similar relationship applies to zeolite bulks, the strength of the ZSM-5 porous bulk body obtained in this study should be comparable to the strength of the ZSM-5 bulk body prepared by Igi *et al.* When comparing the samples with different processes, the strength of the sample (1) was the highest. According to the Weibull's weakest link theory [31], the destruction of ceramics starts from the largest defect. Samples that used starch as a pore-forming agent had a lower strength because they contained macropores which acted as a starting point for the fracture. Since the macropores in the sample (2) are independent, the maximum defect size is small, and as a result, stress concentration during fracture is less likely to occur. This is probably the reason why the compressive strength of the sample (2) was higher than that of the sample (3).

The N₂ gas permeation rate of the bulks is shown in Fig. 11. The sample (3) showed the highest gas permeability among the three, although the sample (2) and the sample (3) indicated almost the same porosity by Archimedes' method. The differences occurred due to the pore structure, the CLFM observation results showed that isolated macropores as large as the starch grains were formed in the sample with unheated starch. The isolated macropores did not contribute to the gas permeability. Spherical pores derived from the starch

irregularly expanded in the heated sample to form a network structure. The increase in the connected structure pores resulted in an increased gas permeation in the sample containing the heated starch. ZSM-5 granules are commonly used as fillers in gas chromatography columns for the purpose of separating inorganic gases. The gas flow rate through the intergranular spaces for that application is approximately 20-30 CCM [32]. On the other hand, the gas flow rate through the continuous macropores in the ZSM-5 bulk body was 2-5 CCM, which was lower than that of gas chromatography. However, the gas flow through the ZSM-5 bulk body can be controlled by optimizing the pore structure according to the amount of starch added and the subsequent treatment conditions. The zeolite bulk body proposed in this study would be applicable for gas treatment purposes.

4. Conclusions

Porous zeolite bulks were fabricated using starch as a pore-forming agent. An X-ray diffraction pattern indicated that the crystal structure of the starting ZSM-5 zeolite material was maintained in the bulk samples through all the processes, implying that the micropores in the zeolite crystal unit were maintained in the bulk bodies. The presence of micropores, mesopores, and macropores in the bulks was suggested by the adsorption / desorption isotherms of N₂ gas. The pore size distribution of the bulk samples had a peak at 7-9 nm, corresponding to mesopores which would be suitable for supporting functional nanoparticles. Changes in the macropore structure due to the starch heating process were confirmed from the cross-sectional images inside the samples observed by confocal laser fluorescence microscopy using the liquid immersion method. The three-dimensional images of macropores created from the cross-sectional images had a higher resolution than

from industrial micro-X-ray computed tomography. This observation method can be applied to other porous materials by properly selecting the refractive index of the immersion liquid. The compressive strength of the zeolite bulk bodies was above 25 MPa, which was higher than the that of general concrete used for construction. This result showed that the bulk bodies had a sufficient mechanical strength for handling. The sample (3) showed the highest gas permeability among the three indicating that the starch networks as pore-forming agents are available to create continuous pore structures for a smooth gas flow.

Acknowledgements

This study was carried out as a part of the France-Japan International Collaboration Framework (IRL3629 LINK). The authors wish to thank Mr. D. Lechevalier of Saint-Gobain KK (Tokyo, Japan) for his significant support involved in LINK and related activities. We also wish to thank Dr. H. Okuyama at NIMS for his help with the experimental setup.

References:

- [1] C. Cundy, P. Cox, The hydrothermal synthesis of zeolites: History and development from the earliest days to the present time, *Chem. Rev.*, 103 (2003) 663-701.
- [2] C. Cundy, P. Cox, The hydrothermal synthesis of zeolites: Precursors, intermediates, and reaction mechanism, *Microporous Mesoporous Mater.*, 82 (2005) 1-78.
- [3] A. Corma, From Microporous to Mesoporous Molecular Sieve Materials and Their Use in Catalysis, *Chem. Rev.*, 97 (1997) 2373-2420.

- [4] J. Jiang, J. Yu, A. Corma, Extra-Large-Pore Zeolites: Bridging the Gap between Micro and Mesoporous Structures, *Angew. Chem. Int. Ed.*, 49 (2010) 3120-3145.
- [5] J. Jiang, Y. Yun, X. Zou, J. Jorda, A. Corma, ITQ-54: a multi-dimensional extra-large pore zeolite with 20 x 14 x 12-ring channels, *Chem. Sci.*, 6 (2015) 480-485.
- [6] J. Sun, C. Bonneau, A. Cantin, A. Corma, M. Diaz-Cabanas, M. Moliner, D. Zhang, M. Li, X. Zou, The ITQ-37 mesoporous chiral zeolite, *Nature*, 458 (2009) 1154-1158.
- [7] L. Bieseki, R. Simancas, J. Jorda, P. Bereciartua, A. Cantin, J. Simancas, S. Pergher, S. Valencia, F. Rey, A. Corma, Synthesis and structure determination via ultra-fast electron diffraction of the new microporous zeolitic germanosilicate ITQ-62, *ChemComm.*, 54 (2018) 2122-2125.
- [8] E. Kapaca, J. Jiang, J. Cho, J. Jorda, M. Diaz-Cabanas, X. Zou, A. Corma, T. Willhammar, Synthesis and Structure of a 22 x 12 x 12 Extra-Large Pore Zeolite ITQ-56 Determined by 3D Electron Diffraction, *J. Am. Chem. Soc.*, 143 (2021) 8713-8719.
- [9] A. Sala, E. Perez-Botella, J. Jorda, A. Cantin, F. Rey, S. Valencia, ITQ-69: A Germanium-Containing Zeolite and its Synthesis, Structure Determination, and Adsorption Properties, *Angew. Chem. Int. Ed.*, 60 (2021) 11745-11750.
- [10] C. Baerlocher, L.B. McCusker, Database of Zeolite Structures, available at <http://www.iza-structure.org/databases/>, (accessed on February 28th, 2022).
- [11] J. Beck, J. Vartuli, W. Roth, M. Leonowicz, C. Kresge, K. Schmitt, C. Chu, D. Olson, E. Sheppard, S. Mccullen, J. Higgins, J. Schlenker, A new family of mesoporous molecular-sieves prepared with liquid-crystal templates, *J. Am. Chem. Soc.*, 114 (1992) 10834-10843.
- [12] C. Kresge, M. Leonowicz, W. Roth, J. Vartuli, J. Beck, Ordered mesoporous molecular-sieves synthesized by a liquid-crystal template mechanism, *Nature*, 359 (1992) 710-712.
- [13] U. Ciesla, F. Schuth, Ordered mesoporous materials, *Microporous Mesoporous Mater.*, 27 (1999) 131-149.

- [14] S. Zou, M. Zhang, S. Mo, H. Cheng, M. Fu, P. Chen, L. Chen, W. Shi, D. Ye, Catalytic Performance of Toluene Combustion over Pt Nanoparticles Supported on Pore-Modified Macro-Meso-Microporous Zeolite Foam, *Nanomater.*, 10 (2020) 30-46.
- [15] M. Anderson, S. Holmes, N. Hanif, C. Cundy, Catalytic Hierarchical pore structures through diatom zeolitization, *Angew. Chem. Int. Ed.*, 39 (2000) 2707-2710.
- [16] E. Igi, Y. Kameshima, S. Nishimoto, M. Miyake, Fabrication of Large Porous ZSM-5 Bulk Bodies by a One-pot Hydrothermal Method, *Chem. Lett.*, 41 (2012) 1414-1416.
- [17] E. Igi, Y. Kameshima, S. Nishimoto, M. Miyake, Separation of alcohol/water mixtures by ZSM-5 bulk bodies prepared with a one-pot hydrothermal method, *Microporous Mesoporous Mater.*, 208 (2015) 160-164.
- [18] S. Hizukuri, K. Ito, I. Maeda, Z. Nikuni, Temperature Dependence of Retrogradation of Starch Pastes, *J. Jpn. Soc. Starch. Sci.*, 19 (1972) 70-75.
- [19] A. Buléon, P. Colonna, V. Planchot, S. Ball, Starch granules: structure and biosynthesis, *Int. J. Biol. Macromol.*, 23 (1998) 85-112.
- [20] K. Ishii, M. Shimizu, H. Sameshima, S. Samitsu, T. Ishigaki, T. Uchikoshi, Fabrication of porous (Ba,Sr)(Co,Fe)O₃-delta (BSCF) ceramics using gelatinization and retrogradation phenomena of starch as pore-forming agent, *Ceram. Int.*, 46 (2020) 13047-13053.
- [21] E. P. Barrett, L. G. Joyner, P. P. Halend, The Determination of Pore Volume and Area Distributions in Porous Substances. I. Computations from Nitrogen Isotherms, *J. Am. Chem. Soc.*, 73 (1951) 373-380.
- [22] M. Thommes, K. Kaneko, A. V. Neimark, J. P. Olivier, F. Rodriguez-Reinoso, J. Rouquerol, K. S.W. Sing, Physisorption of gases, with special reference to the evaluation of surface area and pore size distribution (IUPAC Technical Report), *Pure Appl. Chem.*, 87 (2015) 1051-1069.
- [23] K. Uematsu, Immersion microscopy for detailed characterization of defects in ceramic powders and green bodies, *Powder Technol.*, 88 (1996) 291-298.

- [24] K. Uematsu, Processing defects in ceramic powders and powder compacts, *Adv. Powder Technol.*, 25 (2014) 154-162.
- [25] D. Olson, W. Haag, R. Lago, Chemical and physical-properties of the ZSM-5 substitutional series, *J. Catal.*, 61 (1980) 390-396.
- [26] The Chemical Society of Japan, *Handbook of Chemistry: Pure Chemistry*, 4th ed., Maruzen publishing Co., Japan (1993) II-519.
- [27] Japan Industrial Standards R1608, Testing methods for compressive strength of fine ceramics, Japanese Industrial Standard Committee, Japan, (2003)
- [28] M. A. B. Promentilla, T. Sugiyama, T. Hitomi, N. Takeda, Characterizing the 3D Pore Structure of Hardened Cement Paste with Synchrotron Microtomography, *J. Adv. Concr. Technol.* 6 (2008) 273-286.
- [29] A. Shimizu, T. Noguchi, Outline of Japanese Architectural Standard Specification for Reinforced Concrete Works (JASS 5) -2003, *Concr. J.* 41 (2003) 23-29.
- [30] T. Noguchi, F. Tomosawa, Relationship between compressive strength and various mechanical properties of high strength concrete, *J. Struct. Constr. Eng.*, AIJ 472 (1995) 11-16.
- [31] F. Zok, On weakest link theory and Weibull statistics, *J. Am. Ceram. Soc.* 100 (2017) 1265-1268.
- [32] General Catalog No.30, GL Sciences Inc. (2013) 438.

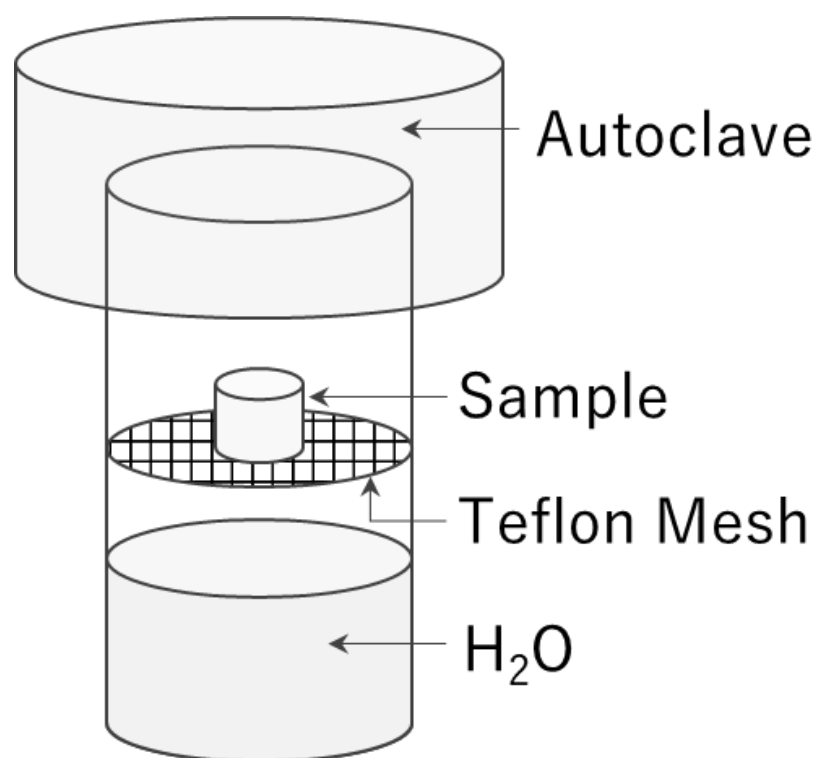


Fig. 1: Schematic illustration of the sample heating process in an autoclave

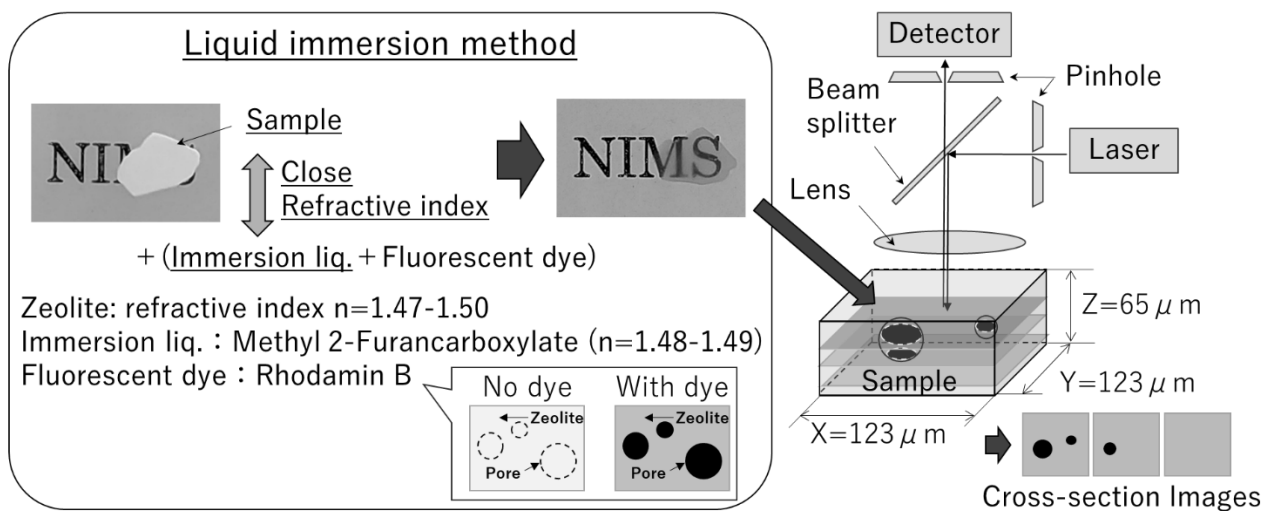


Fig. 2: Observation of pore structure by a confocal laser fluorescent microscope using the liquid immersion method

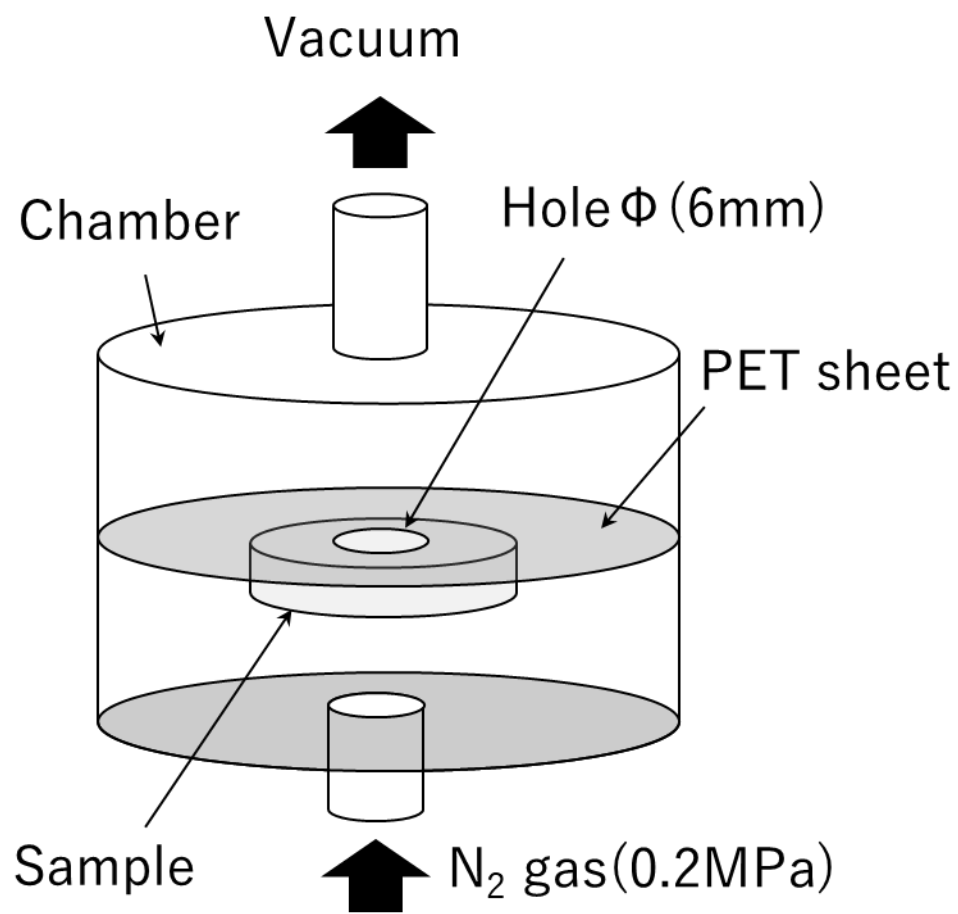


Fig. 3: Schematic illustration of nitrogen gas permeability measurement

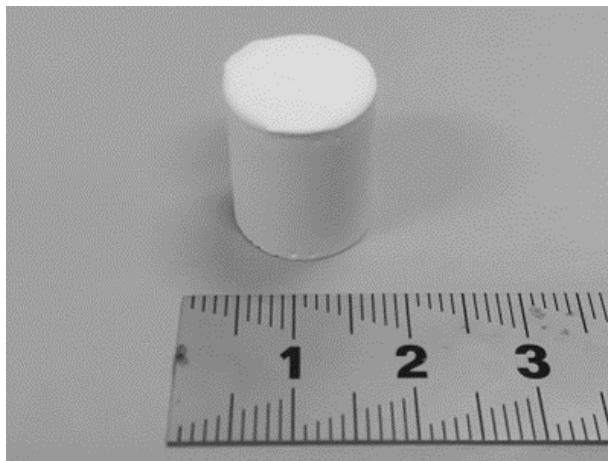


Fig. 4: A zeolite bulk body (sample (3))

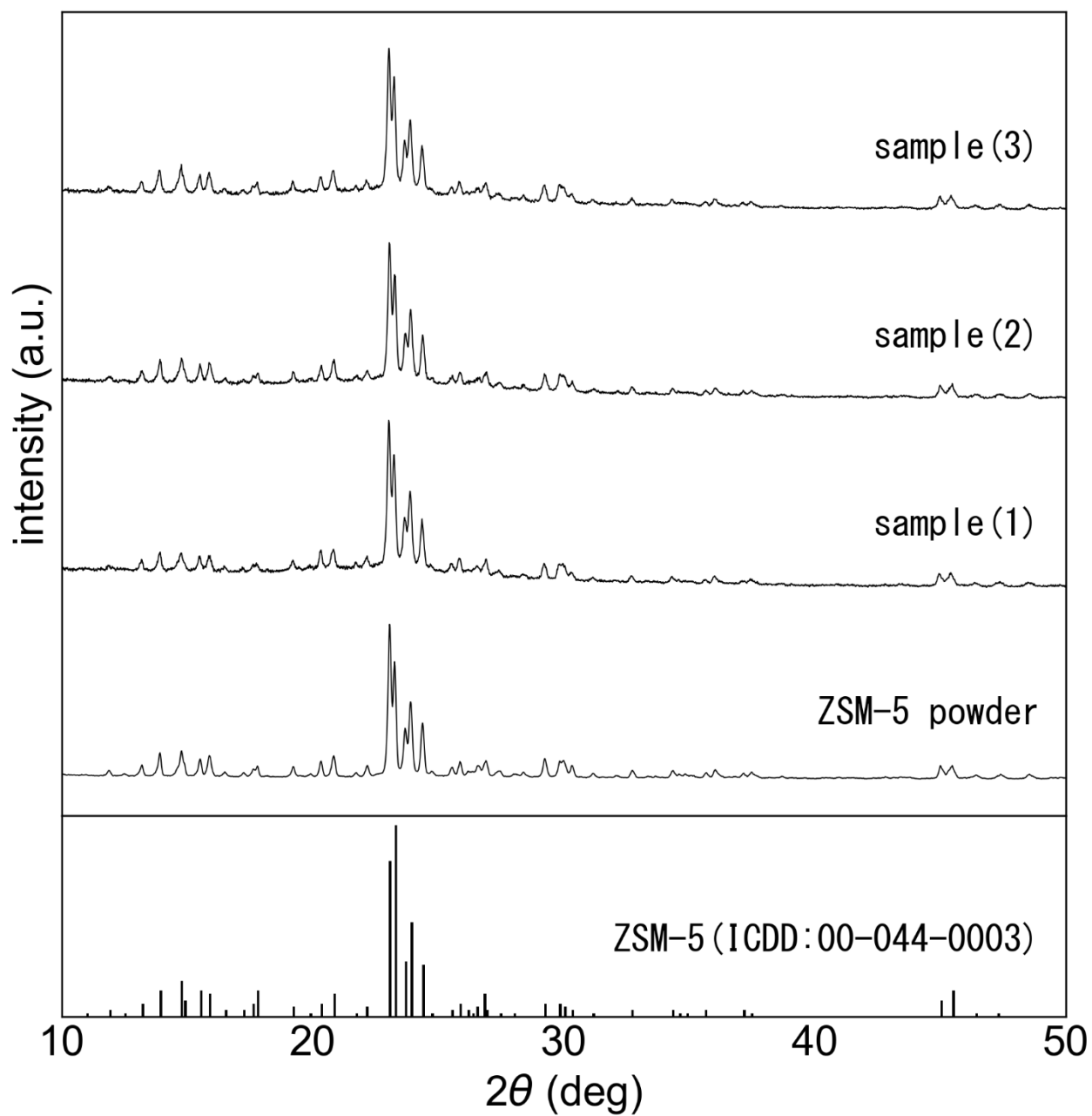


Fig. 5: X-ray diffraction patterns of raw ZSM-5 powder and the bulk samples

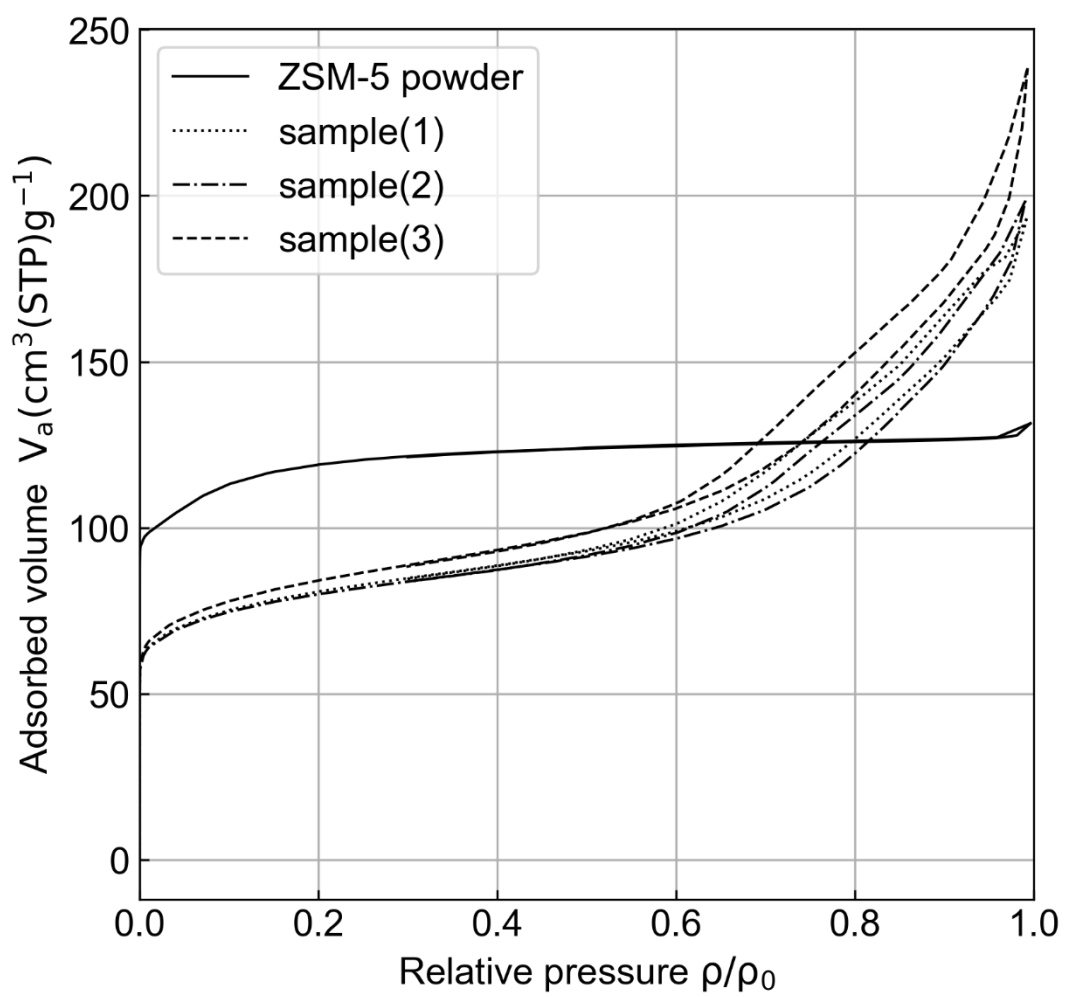


Fig. 6 N₂ adsorption/desorption isotherms measured at 77K

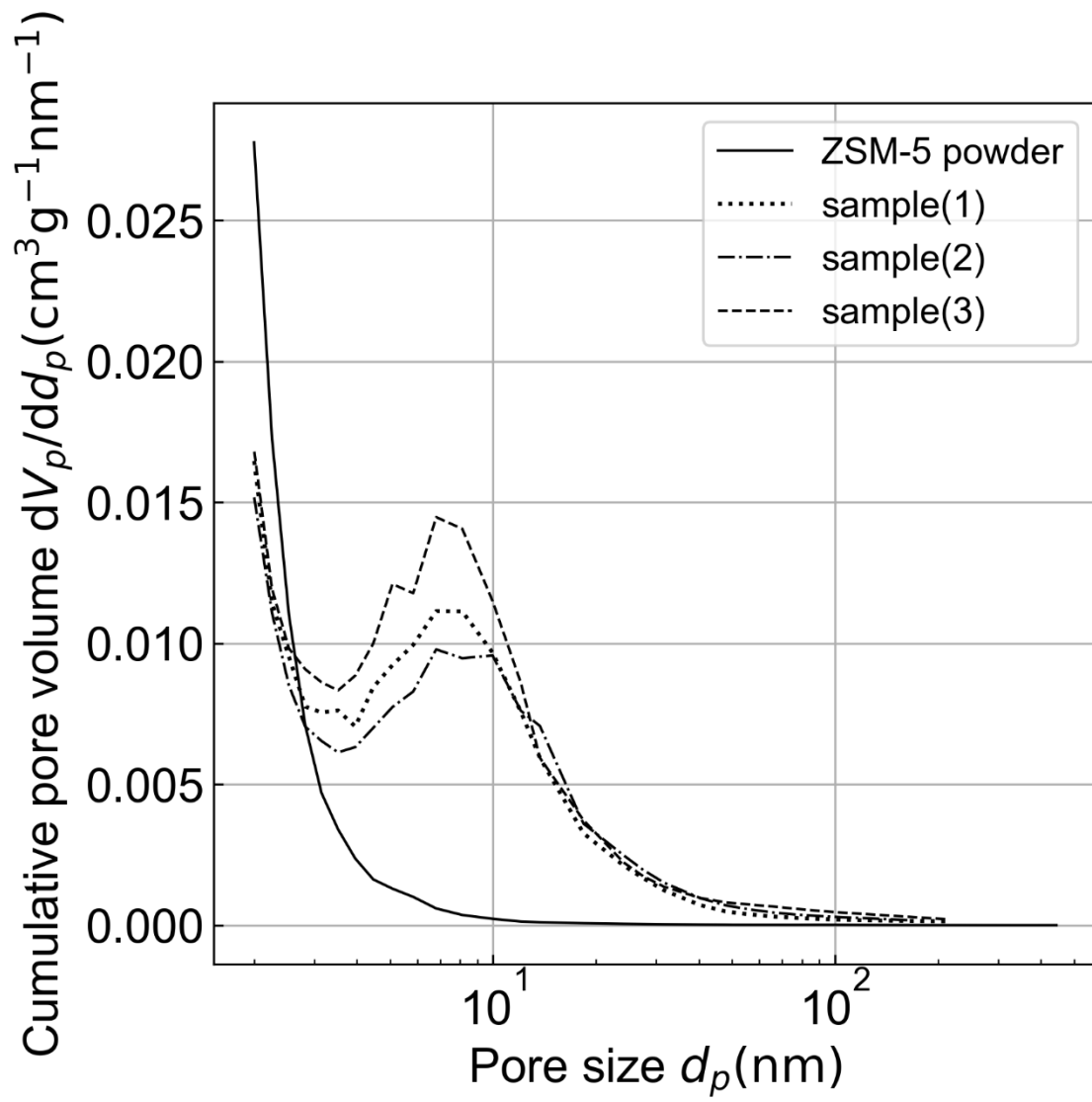


Fig. 7: Pore size distribution obtained from the BJH plots

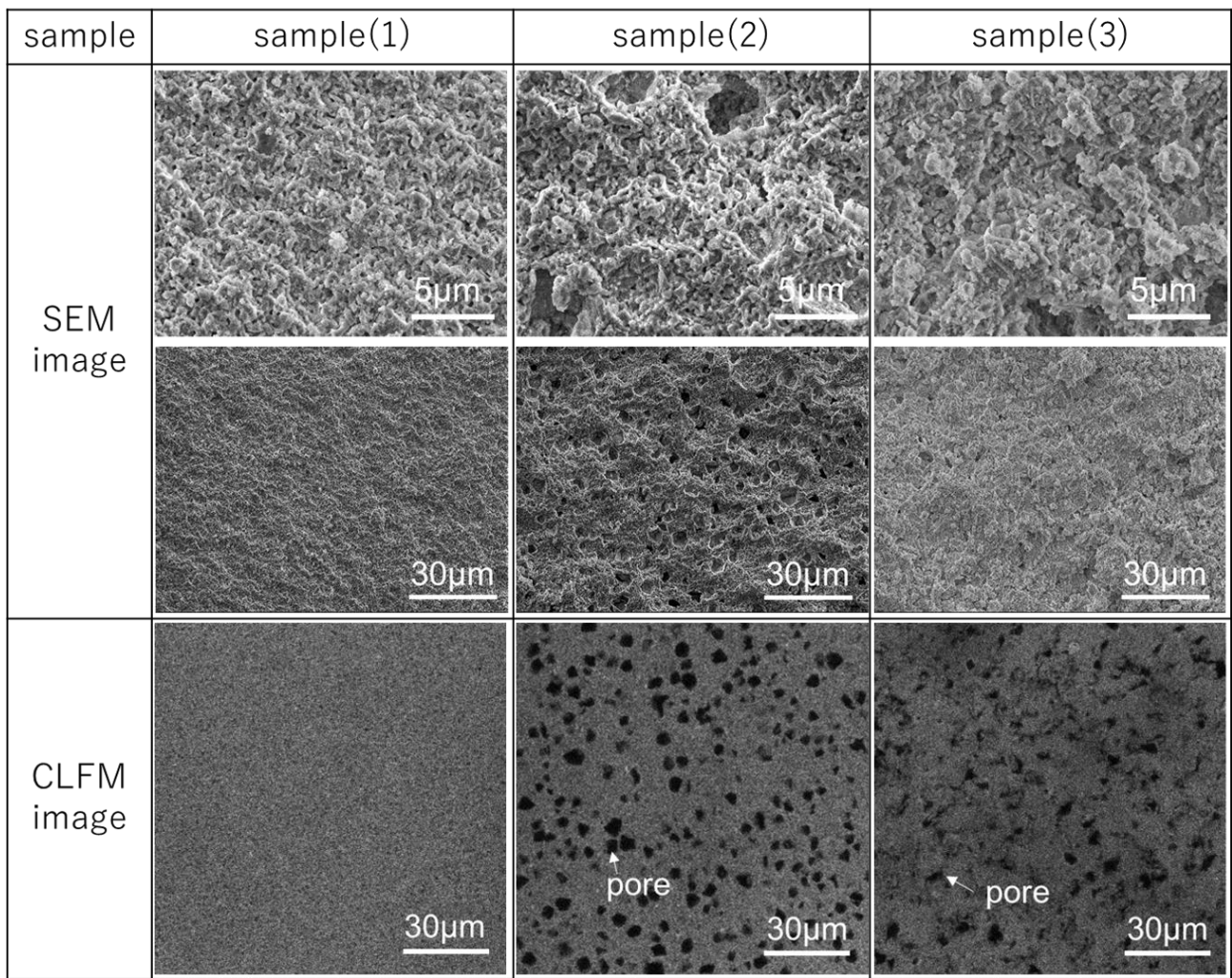


Fig. 8: SEM images of the fracture surface at two different magnifications and CLFM images of the corresponding samples

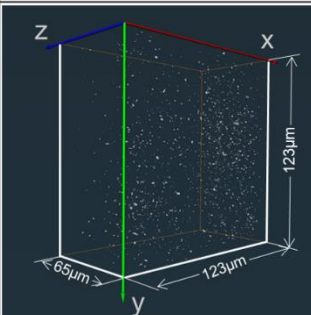
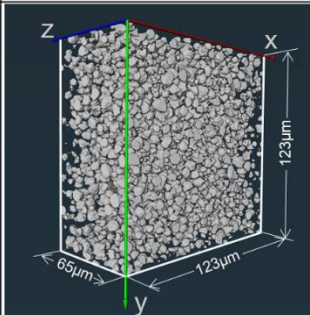
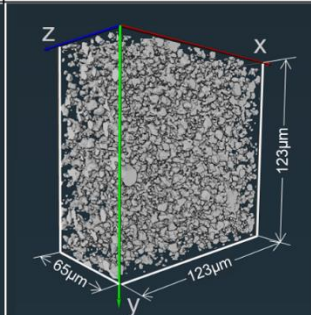
| Sample | sample(1) | sample(2) | sample(3) |
|--|---|--|---|
| Three-dimensional modeling of macropores from CLFM image |  |  |  |

Fig. 9: The three-dimensional images of macropores created from 173 sliced CLFM images

Table 1: Results of density measurement by Archimedes' method

| Sample | sample (1) | sample (2) | sample (3) |
|--------------------------------------|------------|------------|------------|
| Apparent density(g/cm ³) | 2.07 | 2.06 | 2.08 |
| Bulk density(g/cm ³) | 1.36 | 1.12 | 1.13 |
| Porosity (%) | 34.2 | 45.6 | 45.5 |

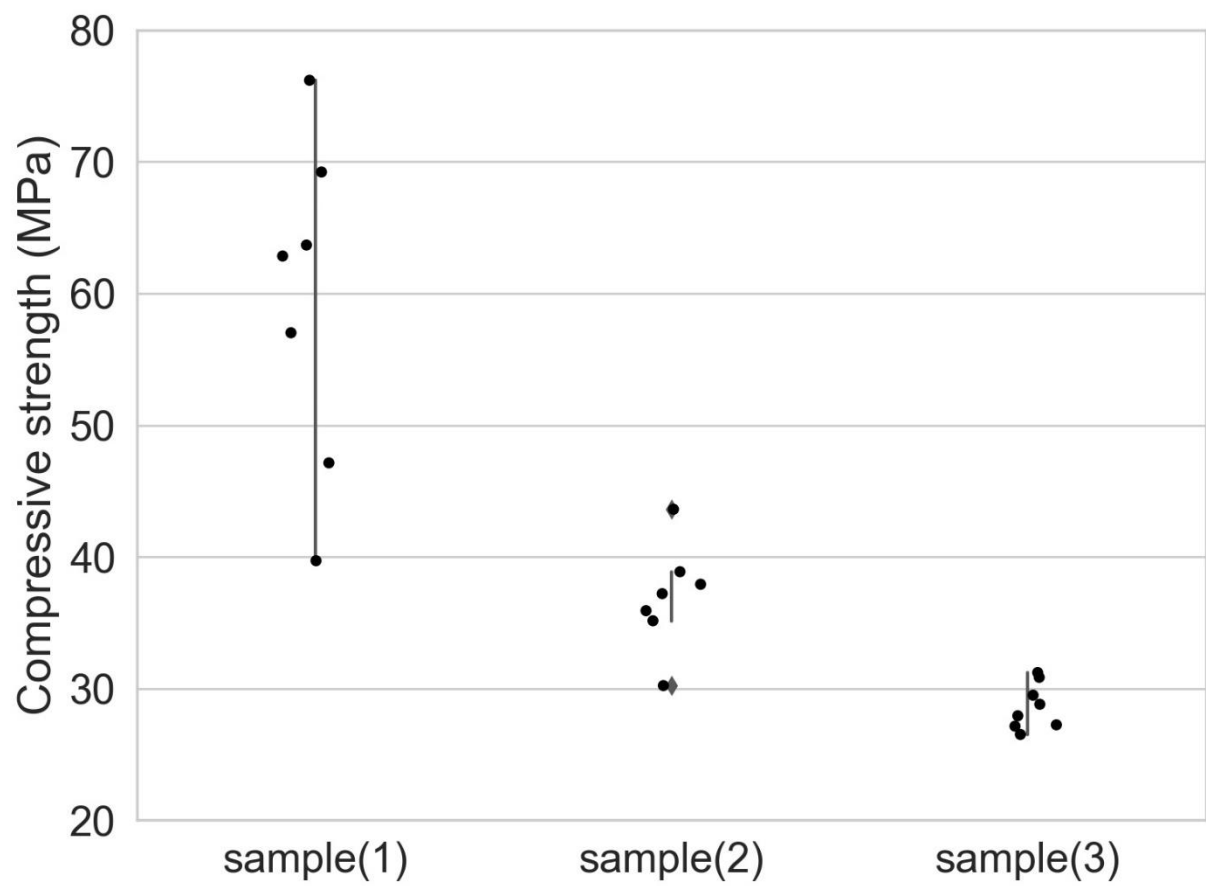


Fig. 10: The compressive strength of the zeolite bulk bodies

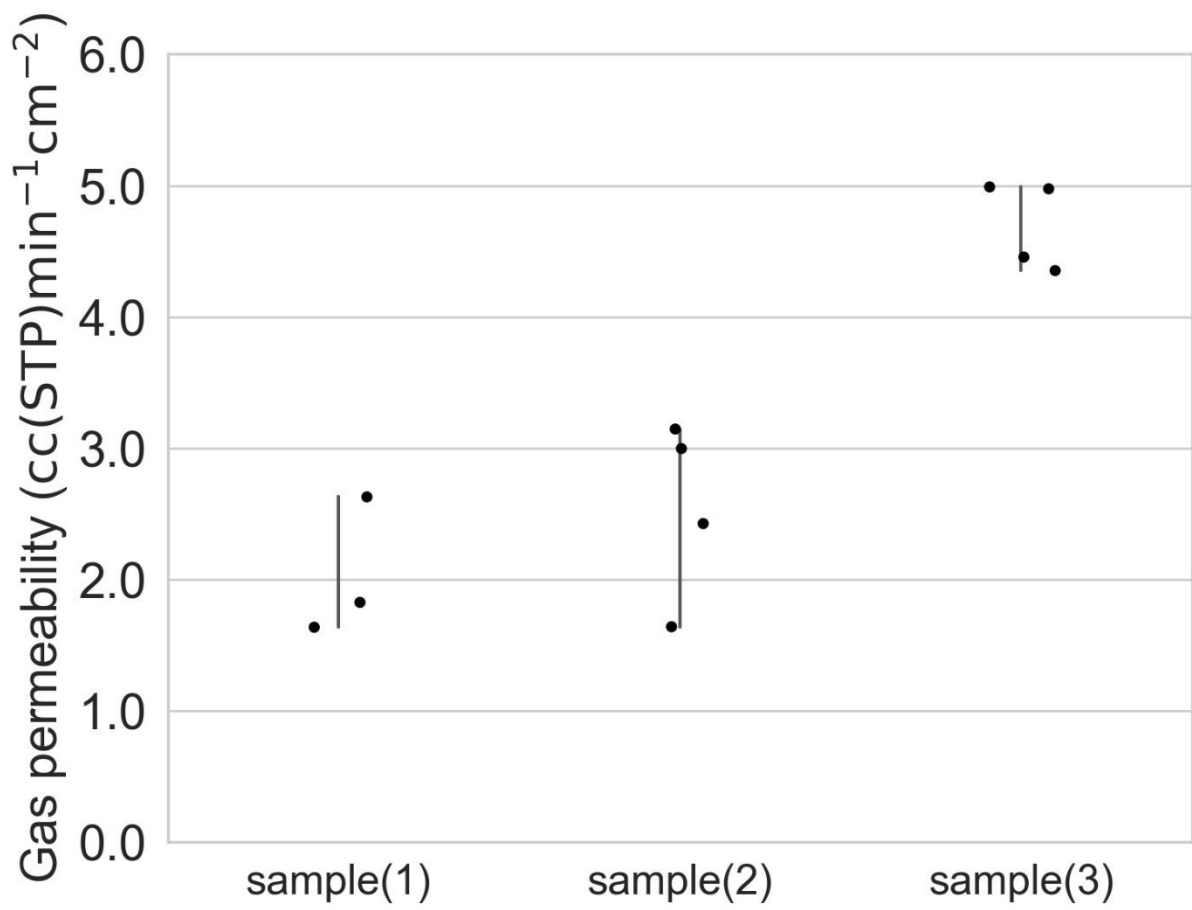


Fig. 11: N₂ gas permeation rate of the bulks

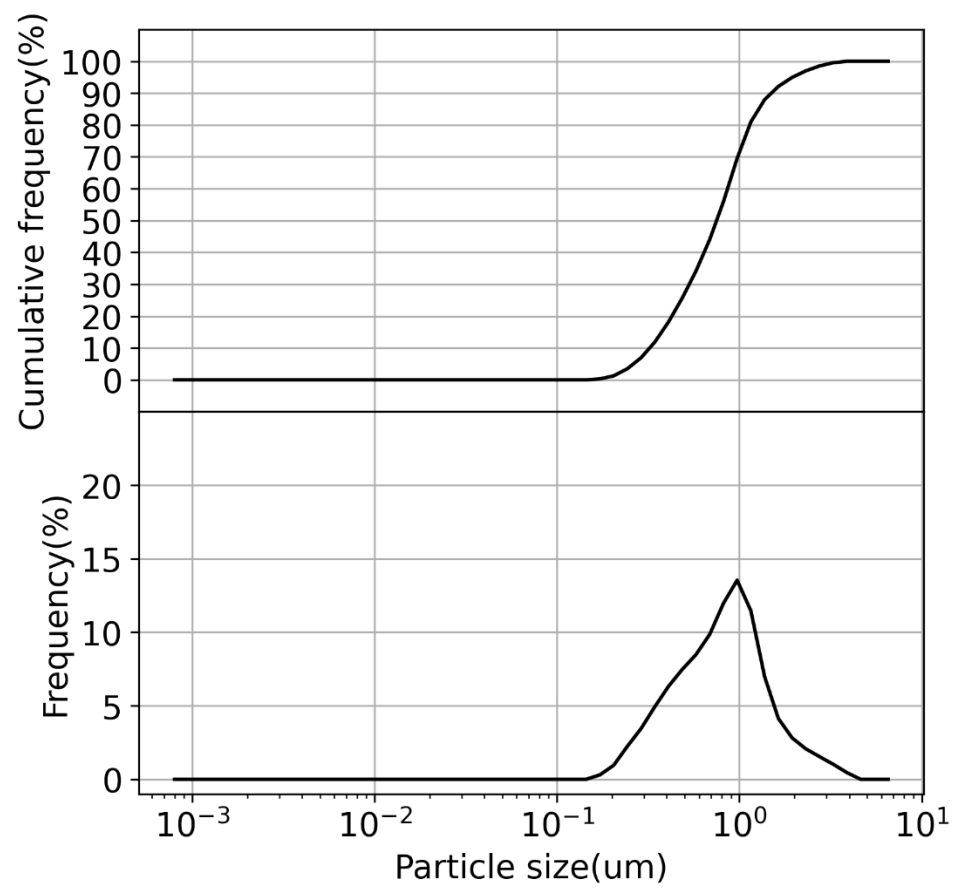


Fig. S1: Particle size distribution of ZSM-5 powder

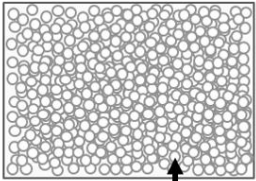
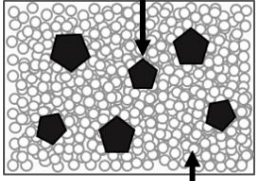
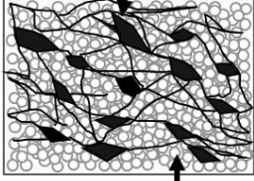
| sample(1) | sample(2) | sample(3) |
|---|--|--|
|  <p>↑ Zeolite particles</p> <p>Sample without starch</p> | <p>Isolated pores</p>  <p>↑ Zeolite particles</p> <p>Sample with starch and no heat-treatment</p> | <p>Connected pores</p>  <p>↑ Zeolite particles</p> <p>Sample with starch and heat-treatment</p> |

Fig. S2: Schematic illustrations of the expected internal structure of each sample